Pharmacological Research 209 (2024) 107444

Contents lists available at ScienceDirect

Pharmacological Research

journal homepage: www.elsevier.com/locate/yphrs

Identification of the TRPA1 cannabinoid-binding site

Tala Amawi [a,1], Alaa Nmarneh [a,1], Gilad Noy [a], Mariana Ghantous [a], Masha Y. Niv [b], Antonella Di Pizio [c,d], Avi Priel [a,*]

[a] The Institute for Drug Research (IDR), School of Pharmacy, Faculty of Medicine, The Hebrew University of Jerusalem, Israel
[b] The Institute of Biochemistry, Food Science and Nutrition, Robert H. Smith Faculty of Agriculture, Food and Environment, The Hebrew University of Jerusalem, Rehovot, Israel
[c] Leibniz Institute for Food Systems Biology at the Technical University of Munich, Freising 85354, Germany
[d] Professorship for Chemoinformatics and Protein Modelling, Department of Molecular Life Sciences, TUM School of Life Sciences, Technical University of Munich, Freising 85354, Germany

ARTICLE INFO

Keywords:
Cannabinoids
Pain
TRPA1
Chemosensors
Binding site

ABSTRACT

Chronic pain accounts for nearly two-thirds of conditions eligible for medical cannabis licenses, yet the mechanisms underlying cannabis-induced analgesia remain poorly understood. The principal phytocannabinoids, the psychoactive Δ^9-tetrahydrocannabinol (THC) and non-psychoactive cannabidiol (CBD), exhibit comparable efficacy in pain management. Notably, THC functions as an agonist of cannabinoid receptor 1 (CB1), whereas CBD shows minimal activity on CB1 and CB2 receptors. Elucidating the molecular targets through which phytocannabinoids modulate the pain system is required for advancing our understanding of the pain pathway and optimizing medical cannabis therapies. Transient receptor potential ankyrin 1 (TRPA1), a pivotal chemosensor in the pain pathway, has been identified as a phytocannabinoid target. Unlike most TRPA1 activators, phytocannabinoid activation is not mediated through the electrophilic binding site, suggesting an alternative mechanism. Here, we identified the human TRPA1 channel cannabinoid-binding site (CBS) and demonstrated that mutations at residue Y840 abolished responses to both THC and CBD at saturating concentrations, indicating a shared primary binding site. Molecular modeling revealed distinct interactions of THC and CBD with the Y840 residue within the CBS. Additionally, CBD binds to the adjacent general anesthetic binding site at oversaturating concentrations. Our findings define the CBS of TRPA1 as overlapping with and adjacent to binding sites for other allosteric activators, suggesting that TRPA1 possesses a highly adaptable domain for binding non-electrophilic activators. This underscores its unique role as a chemosensor in the pain pathway. Furthermore, our results provide new insights into the molecular mechanisms of cannabinoid-induced analgesia and identify novel targets for pain management therapies.

1. Introduction

Chronic pain accounts for nearly two-thirds of the eligible conditions listed in state registries for obtaining a medical cannabis license, making it the primary reason for using medical cannabis [1]. This remarkable use highlights the importance of understanding phytocannabinoids' pharmacological and physiological effects. Cannabis-based medicines approved for medical use include both synthetic variants like dronabinol (Δ^9-tetrahydrocannabinol, THC) and plant-derived options such as Epidiolex (cannabidiol, CBD) [2,3]. These cannabis-based medicines may exert their pain-relieving effects, in part, through interactions with the Transient Receptor Potential (TRP) channels [4,5], a group of ion channels detecting a wide range of physical and chemical stimuli. Several members of this family were shown to be pivotal elements of pain sensation [6–8]. The interaction between cannabinoids and pain system TRP channels represents a complex mechanism by which these

Abbreviation: AITC, allyl isothiocyanate; ARD, ankyrin repeat domain; CBD, cannabidiol; CBG, Cannabigerol; CB1, cannabinoid receptor 1; CB2, cannabinoid receptor 2; CBS, cannabinoid-binding sit; CGRP, calcitonin gene-related peptide; ECS, endocannabinoid system; GA, general anesthetic; PCBs, phytocannabinoids; THC, Δ^9-tetrahydrocannabinol; TRPA1, Transient receptor potential ankyrin 1; VBS, vanilloid binding site. VSLD, voltage-sensor-like domain.

* Correspondence to: School of Pharmacy, Faculty of Medicine, The Hebrew University of Jerusalem, Ein Karem Campus, Jerusalem 9112102, Israel.
E-mail address: avi.priel@mail.huji.ac.il (A. Priel).

[1] These authors contributed equally to this work

https://doi.org/10.1016/j.phrs.2024.107444
Received 16 June 2024; Received in revised form 29 September 2024; Accepted 29 September 2024
Available online 4 October 2024

compounds can alleviate pain, offering potential therapeutic targets for the development of novel pain management strategies. CBD has been shown to modulate TRPA1, TRPV1–4, and TRPM8. THC, on the other hand, does not directly affect the TRPV1 activity and was shown to date to only activate TRPA1 channels [2,5,9,10]. Nevertheless, although phytocannabinoids were used to clone the TRPA1 channel [11], the exact activation mechanism and the cannabinoids binding site (CBS) are yet to be defined.

TRPA1 ion channel, cloned two decades ago [11,12], is the only member of the TRPA subfamily. It is a Ca^{2+} permeable non-selective cation channel predominantly expressed in sensory neurons and co-localized with pain biomarkers such as the TRPV1 and calcitonin gene-related peptide (CGRP) [13]. TRPA1 plays critical physiological processes that involve nociception, mechanotransduction, thermal, and oxygen sensing, and it is considered one of the primary chemosensors of the pain pathway [14,15]. Multiple compounds, including exogenous irritants and endogenous products of tissue injury and inflammation, activate this channel [13,16–19]. TRPA1 detects a wide range of environmental and endogenous electrophilic irritants, which activate the channel through covalent modification of cytoplasmic cysteine residues in the pre-S1 and ankyrin repeat domain (ARD) [20]. Mutations of these three amino acids (C621S, C641S, C665S in the human gene) lead to the collapse of this site, making the channel unresponsive to electrophilic agonists; however, the channel remains functional, with slightly reduced ion permeability [20–22]. Unlike most other agonists, phytocannabinoids do not interact with the channel through a covalent, cysteine-dependent method, and their action is independent of cellular content [21]. Several cannabinoids, including CBD, THC, and Cannabigerol (CBG), were shown to activate TRPA1 robustly [2,5,9,10]. Activation by non-electrophilic agonists has been less studied, and a few distinct binding pockets have been identified. Most non-electrophilic binding sites have been identified by comparing species-specific differences [22,23]. To date, all TRPA1 non-electrophilic binding sites fit the flexible pore vestibule. The most studied binding pocket was for the antagonist A-967079, revealed through species-specific differences and validated by cryo-EM structure [24,25]. A-967079 is a potent antagonist that blocks channel gating by binding to S5, S6, and pore helix 1 [24–27]. Later studies have identified the S5/S6 domain as a target region for hydrophobic and non-electrophilic agonists such as a general anesthetic (e.g., propofol) [21,27–29]. Another binding site for a new synthetic noncovalent agonist, GNE551, was recently reported and confirmed with the cryo-EM structure of the TRPA1-GNE551 complex [30]. This binding pocket is formed by the voltage-sensor-like domain (VSLD; S1–S4) of one subunit and the pore domain (S5–S6 helices) of the neighboring subunit and was characterized as a hydrophobic pocket [30].

The present study aims to define the activation mechanism(s) of TRPA1 by phytocannabinoids. Initial screening of known human TRPA1 (hTRPA1) binding sites has uncovered intriguing insights. Our findings suggest that CBD and THC directly interact with the Y840 residue. Using molecular modeling of the previously published hTRPA1-GNE551 complex, we show that the investigated cannabinoids have a distinct pose in this binding site. Surprisingly, we found that only CBD at high concentrations binds also to the general anesthetic binding site. This complexity suggests that CBD's interaction with TRPA1 may involve multiple binding domains, contributing to its diverse therapeutic effects [31]. Our combined experimental and computational results suggest that the prominent cannabinoid binding site (CBS) of TRPA1 is found in the interface between S4 of one subunit and S5 of the neighboring subunit. Also, the general anesthetic binding site may serve as a binding domain for certain cannabinoids (e.g., CBD) but with lower affinity and efficacy. Thus, these data explain TRPA1 activation by natural non-electrophilic compounds, which evolved to interact specifically with this receptor. Also, our data emphasize TRPA1's role as a pivotal chemosensor of the pain pathway. Moreover, our findings may serve as a structural basis for the rational design of cannabinoid-based analgesics.

2. Materials and methods

2.1. Sub-cloning and site-directed mutagenesis

The human Transient Receptor Potential Ankyrin 1 (hTRPA1) gene, obtained from OriGene Technologies, was subcloned into the pCDNA3.1+ vector, utilizing the Phusion High-Fidelity DNA Polymerase and T4 ligase enzymes (New England Biolabs). Site-directed mutagenesis was performed on hTRPA1 using the Quickchange lightning multi-site-directed mutagenesis kit (Agilent cat. no. 210513–5) or the Q5 Site Mutagenesis Kit (New England Biolabs cat. no. M0494S) according to the manufacturer's protocols. Primers were designed using the Quickchange primer design by Agilent or the NEBaseChanger by New England Biolabs and synthesized by Sigma Aldrich (Suppl. Table 1). DNA constructs were extracted from XL-10 Gold (Agilent) using a miniprep kit (Nucleospin plasmid, Macherey-Nagel) according to the manufacturer's protocol. All constructs were verified by complete gene sequencing (Hy Labs).

2.2. Cell culture and transient transfection

Human embryonic kidney 293 T (HEK293T) (ATCC, CRL-3216) cells were cultured in Dulbecco's modified Eagle's medium (DMEM, Gibco, Thermo Fisher Scientific) supplemented with 10 % fetal bovine serum (Gibco, Thermo Fisher Scientific), 1 % Penicillin-Streptomycin (Gibco, Thermo Fisher Scientific), and 25 mM HEPES (Gibco, Thermo Fisher Scientific) (pH-7.3). Cells were grown at 37 ºC and 5 % CO2; Cells were passaged twice weekly (up to 15 passages) as previously described [32]. Cell transfection was carried out as follows: HEK293T cells were transfected with 1 μg of total DNA (for calcium imaging: 0.4 μg of wt or mutated hTRPA1 in pCDNA3.1+ and 0.6 μg pCDNA3.1+; for electrophysiological analysis: 0.4 μg of wt or mutated hTRPA1 in pCDNA3.1+, 0.4 μg EGFP pCDNA3.1+, and 0.2 μg pCDNA3.1+) using Mirus LT1 transfection reagent (Mirus Bio) or Lipofectamine 3000 (Thermo Fisher Scientific) with Opti-MEM I Reduced Serum Medium (Invitrogen) according to manufacturers' protocol. Transfections were performed in 12-well plates containing ~3×10^5 cells 24 h before analysis. Cells were plated on 0.1 mg/ml PDL (Corning)-coated glass coverslips (12 mm) or coated imaging chambers (μ-slide, 8 well, Ibidi) and incubated at 37 °C (5 % CO2) for at least two hours before electrophysiological and 30–40 min before calcium imaging analysis.

2.3. Live-cell calcium imaging

Live-cell calcium imaging was performed as previously described [33]. Briefly, hTRPA1 transfected HEK293T cells were spotted at Poly-D-Lysine (PDL, 0.1 mg/ml) coated imaging chambers (μ-slide, 8 well, Ibidi) and incubated for 30–40 min in a humidified incubator at 37 °C and 5 % CO_2 before being loaded with 5 μM/ml Fura-2 AM (cat. no. F1201, Invitrogen) dissolved in Ringer's solution (in mM: 140 NaCl, 2.5 KCl, 1.8 $CaCl_2$, 2 $MgSO_4$, 20 HEPES and 5 D-glucose, pH 7.4 with NaOH) supplemented with Pluronic F-127 acid (0.01 %; Sigma-Aldrich) and incubated for 1 hr in the dark at RT. After loading, cells were washed twice with Ringer's solution and incubated for 15 min in the dark at RT. Stock solutions in DMSO or ethanol were dissolved in Ringer's solution to desired concentrations. Using an inverted microscope (IX71, Olympus), cells were illuminated with a xenon arc lamp, and excitation wavelengths (340/380 nm) were selected by a Lambda DG-4 monochromatic wavelength changer (Sutter Instrument). Intracellular Ca^{2+} concentration was measured by digital video microfluorometry with a front-illuminated interline CCD camera (ORCA-FLASH4.0LTPlusDigital, Hamamatsu) using MetaFluor fluorescence ratio imaging software (Molecular Devices). Dual images (340 and 380 nm excitation, 510 nm emission) were collected, and pseudocolor ratio-metric images were monitored every 4 s during the experiment. Data analysis was performed with MetaFluor fluorescence ratio imaging software offline. All

experiments were carried out at room temperature.

2.4. Electrophysiology

Patch-clamp recordings from transfected HEK293T cells in the whole-cell configuration were performed using an Axopatch 200B patch-clamp amplifier (Molecular Devices). Membrane currents were digitized using a Digidata 1440 A interface board and pCLAMP 10.7 software (Molecular Devices) with a sampling frequency set to 5 kHz and low-pass filtered at 2 kHz as previously described [32,34]. The holding voltage was −40 mV. Patch electrodes were fabricated from borosilicate glass using the P1000 Micropipette Puller (Sutter Instrument) and fire-polished using the microforge MF-900 (Narishige) to the resistance of 2–4 MΩ. The standard pipette solution contained 130 mM $CsMeSO_4$, 15 mM CsCl, 5 mM EGTA, 10 mM HEPES, and 2 mM MgATP, adjusted to pH 7.3 with CsOH. The bath solution contained (mM) 140 NaCl, 2.8 KCl, 2 $MgSO_4$, 5 MES, and 5 HEPES and was adjusted to pH 7.4 with NaOH. Solutions containing different modulators and inhibitors were made by adding an appropriate amount of the compound to a bath solution to obtain a working solution. After establishing the whole-cell configuration, ramps (1 s^{-1}) were administrated from −80 mv to + 80 mv, and cells were perfused using the ValveBank perfusion system (AutoMate Scientific). All experiments were carried out at room temperature.

2.5. Molecular modeling

2D structures of THC and CBD were downloaded from PubChem. Ligprep (Schrödinger Release 2023–3: LigPrep, Schrödinger, LLC, New York, NY, 2023) was used to generate 3D structures and protonation states of the ligands at pH 7 ± 1. The TRPA1 structure with PDB ID: 6X2J [30] was prepared with the Protein Preparation Wizard tool available in Maestro (Schrödinger Release 2023–3). Induced Fit Docking (Schrödinger Release 2023–3: Glide and Prime, Schrödinger, LLC, New York, NY, 2023) simulations were performed to investigate the binding modes of THC and CBD in the GNE551 binding site and the general anesthetics binding site. The center of the box was set within the centroid of residues S873, T874, M912, and M953 for the general anesthetic binding site and in the centroid of the ligand in PDB structure 6X2J for the GNE551 binding site. Using the Ligand Interaction Diagram tool available in Maestro (Schrödinger Release 2023–3), we mapped the residues at 4 Å from the ligands in the general anesthetic (GA) and GNE551 binding sites.

2.6. Chemicals

All salts and buffers were purchased from Sigma-Aldrich. All drugs were dissolved according to manufacturer protocol. Δ^9-Tetrahydrocannabinol (THC), and Cannabidiol (CBD), were purchased from THC Pharm, and Cannabigerol (CBG) was purchased from Symrise. Cannabinoids were weighed and immediately dissolved in DMSO or ethanol to 20–100 mM and diluted in either Ringer's or bath solution containing Pluronic F-127 (0.01 %) to achieve the desired working concentration. Allyl isothiocyanate (AITC) and Pluronic F-127 were purchased from Sigma-Aldrich. Fura-2 AM was purchased from Invitrogen.

2.7. Statistics and reproducibility

We assumed a normal distribution for our data but did not formally check it. The sample size (n) indicates the number of individual cells or experiments replicated, as pointed out. Transfected cells from at least three different transfections per construct were used to account for potential day-to-day variation. Results are presented as mean ± SEM if not stated otherwise, but individual data points are shown in the figures, allowing for visual assessment of data variation. P values were calculated using unpaired t-tests for between comparisons involving two groups. For analyses concerning multiple groups, one or two-way ANOVA was used according to the number of independent variables or factors being analyzed, followed by Tukey or Dunnett's post hoc tests as appropriate.

All statistical data were analyzed using Prism 10 software (GraphPad Software, CA, USA).

Electrophysiological analysis was performed using pCLAMP 10.7 software (Molecular Devices, CA, USA). Calcium imaging analysis was performed using MetaFluor Fluorescence Imaging Software (Molecular Devices, CA, USA). Dose-response curves were calculated using Prism 10 (GraphPad Software, CA, USA) software.

The sigmoidal Hill equation is as follows:

$$\frac{I}{I_{max}} = \frac{[X]^n}{EC_{50}{}^n + [X]^n}$$

Where: I = measured current/ calcium response, Imax = maximal current/ calcium response at a saturating dose (pre-measured for each construct), x = tested agonist concentration, EC_{50} = the calculated concentration elicits 50 % of maximal current, and n = Hill coefficient.

3. Results

3.1. Phytocannabinoids (PCBs) have distinct TRPA1 activation profile

To identify the putative TRPA1 cannabinoid binding site (CBS), we first ask which phytocannabinoids (PCBs) have the highest efficacy and potency. This analysis is important because using mutagenesis analysis may hamper the gating properties of the channel; thus, weak agonists may lead to false positive conclusions. Previous studies demonstrate that many PCBs activate TRPA1 with different pharmacological profiles [9]. Hence, we define the dose-response of the most abundant cannabinoids in the cannabis plant [35,36]. using calcium imaging of transiently expressed human TRPA1 (hTRPA1) in HEK293T cells (Fig. 1A & B). We compared the PCBs response to the canonical electrophilic agonist allyl isothiocyanate (AITC) [31,37]. While we could not establish a complete dose response for Cannabigerol (CBG) (due to salting out of the compounds in high concentrations), Δ^9-tetrahydrocannabinol (THC) and Cannabidiol (CBD) demonstrate similar potency and efficacy as AITC (Fig. 1B & Suppl. Fig. 1A). To verify these findings, we recorded the THC- and CBD-evoked hTRPA1 currents (Fig. 1C), and determine their dose-response (Fig. 1D). We used the whole-cell configuration of the patch clamp technique and recoded the response at membrane potential of −40 mV to mimic the calcium imaging conditions. In parallel, we also recorded the response of hTRPA1 to THC, CBD, and CBG using voltage ramps (−80 mV to +80 mV) as commonly done for TRPA1 (Suppl. Fig. 1B-E) [38,39]. Our results suggest that THC and CBD were the most potent and efficacious PCBs, and THC demonstrated better efficacy than CBD (Fig. 1D).

The relatively fast washout of the PCBs-evoked hTRPA1 currents (Fig. 1C) and the study by Hinman et al. [20] show that THC activation is independent of the electrophilic binding sites, suggesting that PCBs are non-electrophilic activators of TRPA1 with reversible binding. To verify that PCBs do not activate TRPA1 through covalent bonds with the cysteines in the electrophilic binding site, we analyzed the response of the triple cysteine mutant receptor (hTRPA1(3 C; C621S, C641S and C665S)) to PCBs and the electrophilic agonist AITC. While the AITC response was abolished, the PCB's response remained intact (Fig. 1E-F, and Suppl. Fig. 1F). Hence, PCBs are potent and efficacious TRPA1 non-electrophilic agonists that do not depend on the electrophilic binding site.

3.2. THC and CBD have a distinct activation mechanism

To define the binding site of PCBs, we analyzed the main residues previously suggested to participate in the binding of non-electrophilic agonists and antagonists. Of note, both cryo-EM structures and

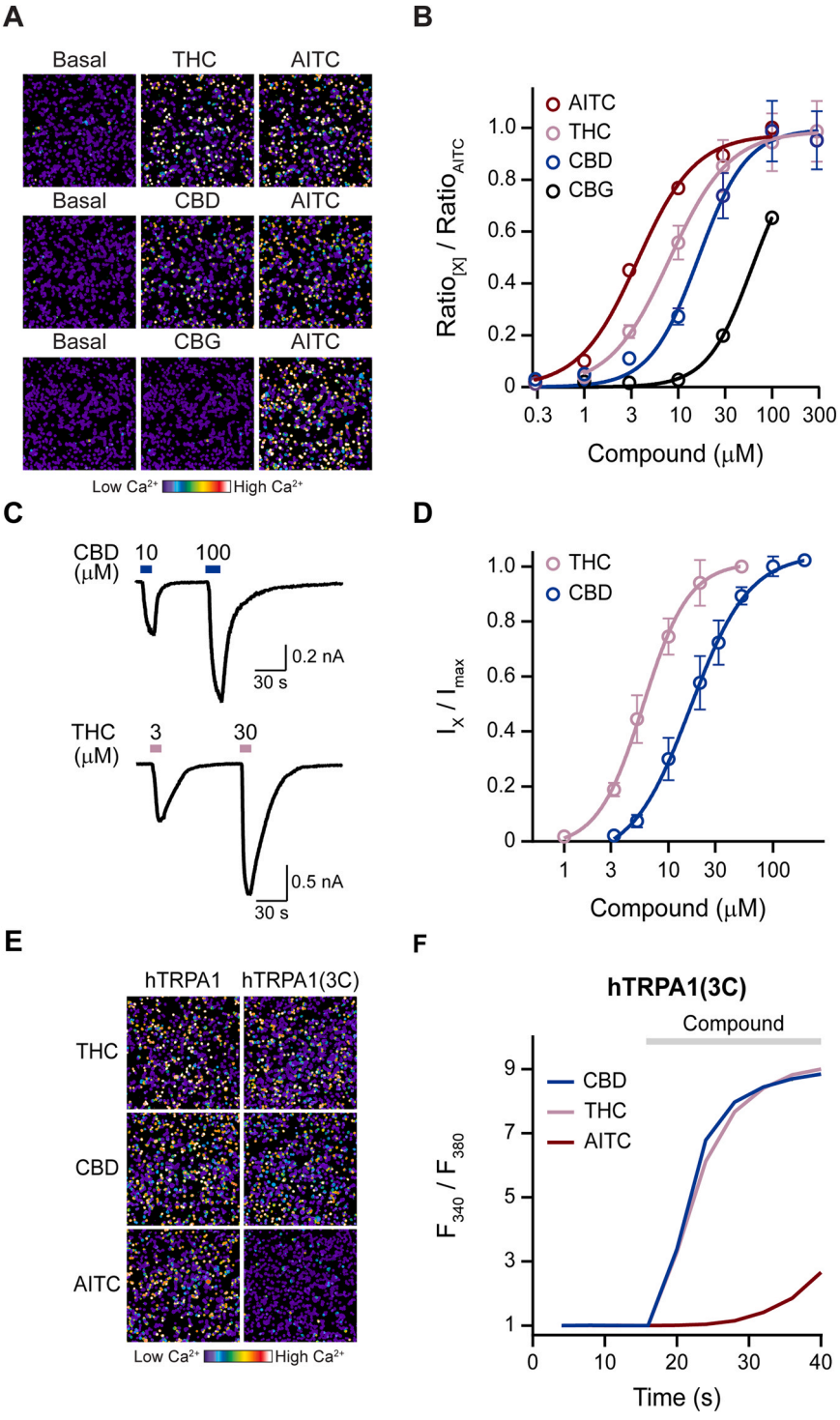

(caption on next page)

Fig. 1. CBD and THC are non-electrophilic TRPA1 agonists. A. Representative pseudo-colored images of HEK293T cells transiently expressing hTRPA1 after applying 10 μM of THC (**top panels**), CBD (**middle panels**), and CBG (**bottom panels**) followed by applying AITC (100 μM). The scale bar indicates levels of intracellular calcium. **B.** Normalized concentration-response relationship analysis for different PCBs (THC, CBD, and CBG) and AITC. As shown in **A**. Each point represents a mean (± SEM) response of an average of 150–300 HEK293T cells transiently expressing hTRPA1; Solid lines fit the Hill equation. AITC (dark red line, EC_{50} = 3.68 ±0.10 μM; n_H =1.40±0.04); THC (light pink line, EC_{50} = 8.10 ±1.97 μM; n_H=1.36±0.37); CBD (blue line, EC_{50} = 16.40 ±2.98 μM; n_H =1.67±0.42); and CBG (black line, EC_{50} = 61.06 ±16.02 μM, n_H =1.81±0.31) as determined by live-cell calcium imaging (as shown in A). Values are normalized to 100 μM AITC evoked responses. **C.** Representative whole-cell current traces (V_m = −40 mV) from HEK293T cells transiently expressing hTRPA1 after application of CBD (10 μM and 100 μM respectively, blue bars; top panel) or application of THC (3 μM and 30 μM respectively, light pink bars; bottom panel). Note that the currents are washed upon removal of either CBD or THC. **D.** Normalized concentration-response relationships to THC and CBD as determined by whole-cell recordings (as done in C). Each point represents the average (± SEM) response of 5–8 cells. Solid lines fit the Hill equation. THC (light pink line, EC_{50} = 5.74 ±0.82 μM; n_H=1.9±0.54); CBD (blue line, EC_{50} = 16.22 ±3.88 μM; n_H=1.6±0.58). **E.** Representative pseudo-colored images of HEK293T cells transiently expressing wt hTRPA1(**left panels**) and the electrophilic-binding site mutated receptor hTRPA1(3 C) (**right panels**) after application of THC (100 μM) or CBD (100 μM), or AITC (30 μM). The scale bar indicates levels of intracellular calcium. **F.** Changes with time of intracellular calcium levels of HEK293T cells expressing the electrophilic-binding site mutated receptor hTRPA1(3 C) in response to different applications of PCBs; THC, (100 μM, light pink line), CBD, (100 μM, blue line) or the application of AITC (30 μM, dark red line) as determined by live-cell calcium imaging. The scale bar indicates the application time and duration (compound, grey bar). All graphs represent the mean of 3–4 independent experiments (each 50–100 cells). Note that the PCBs response is not affected by the mutations of the electrophilic binding site.

mutagenesis analysis point to the S5-S6 region as the non-electrophilic binding domain [25–28]. Hence, several residues in this region participate in the binding of multiple agonists and antagonists. Using calcium imaging, we tested ten hTRPA1 mutated receptors previously shown to interact with different ligands directly (Fig. 2A). Including the F909T, F944A, and L881I mutants shown to be part of the antagonist A967079 binding site [17,25,40]; S873V, T874L, S873V/T874L, and V875G mutants shown to be part of the agonist's menthol, thymol, carvacrol binding site [17,28,41,42]; S873V, T874L, S873V/T874L, M912A and M953A mutants shown to be part of the general anesthetics activation and binding sites [17,27,42]; S873V, and Y840W mutants shown to be part of the agonist β-eudesmol binding site [43]; Y840W mutant shown to be part of the agonist GNE551 binding site [30]. We examined the sensitivity of both THC (Fig. 2B & C) and CBD (Fig. 2D & E).

Surprisingly, while the Y840W mutation was sufficient to abolish the THC response, the CBD response was significantly reduced by each of the mutants: S873V, M953A, and Y840W (compare Figs. 2C to 2E). Of note, unlike M953A and Y840W, S873V demonstrates low expression levels (compare Fig. 2 to Suppl. Fig. 2A-B). To verify that these mutations do not hamper the gating mechanism of TRPA1, we examined whether these mutations affect the response of the canonical electrophilic AITC. We found that S873V altered the AITC response (Suppl. Fig. 2C). However, the AITC response for both Y840W and M953A remained similar to the wt hTRPA1 receptor (Suppl. Fig. 2C). Thus, our results suggest that while CBD activation requires at least two binding domains, THC binds and activates TRPA1 through the GNE551 and β-eudesmol binding domain.

3.3. THC and CBD activate TRPA1 through the suggested GNE551 and β-eudesmol binding site

To analyze the THC and CBD binding to the previously suggested GNE551 and β-eudesmol binding site [30,43], we generated a series of mutated TRPA1 at residues that were shown to be part of the GNE551 binding pocket according to the cryo-EM structure (Fig. 3) [30]. Interestingly, we found that most of the mutations that significantly hampered the GNE551 binding dramatically reduced the THC and CBD-evoked TRPA1 activation (Fig. 3B & 3D). Of note, the mutation S887W hampered the AITC response and was excluded from further analysis (Fig. 3A & C). While the mutations Y840W and Q940V were shown to abolish the GNE551 response [30], only the Y840W abolishes both the THC and CBD response (Fig. 3). To test whether residue Q940 is part of the cannabinoid binding site, we mutated it to several amino acids representing changes in size, rigidity, hydrophobicity, and polarity (Suppl. Fig. 3A-B). All the aromatic residues significantly reduce the THC and CBD response. However, all the other mutations in this position affect only the THC binding (Suppl. Fig. 3A-B). Hence, our results demonstrate that TRPA1 activation by THC and CBD requires Q940, similar to the GNE551, but with different interactions. To test whether the dramatic effect of Q940W compared to other Q940 substitutions results from hampering channel activity, we analyzed the AITC and CBD-evoked current of wt hTRPA1 and Q940W receptors. While the CBD response of Q940W was significantly hampered, the AITC response was intact (Suppl. Fig. 3C-D). Thus, our mutation analysis demonstrates that the suggested synthetic compound binding site (i.e., GNE551) also binds the natural cannabinoids THC and CBD.

Next, using Induced-Fit docking, we examine the possible interaction of THC (Fig. 4A) and CBD (Fig. 4B) with residues in the GNE551 binding site according to the published cryo-EM structure of GNE551 bound to the hTRPA1 receptor [30]. According to our model, Y840 directly interacts with both cannabinoids; however, each cannabinoid generates a different interaction type with this residue. While in THC, the aromatic ring forms π-π stacking with the aromatic ring of Y840, CBD forms hydrogen bonds between its hydroxyl group and the Y840 hydroxyl. To test our binding model, we performed a mutagenesis analysis of the Y840 residue (Fig. 4C & 4D). As expected from our docking, substitution to phenylalanine (benzyl side chain) hampered the CBD interaction with minimal effect on THC (Fig. 4C & 4D). To verify our calcium imaging results that the Y840F has minimal effect on the interaction with THC, we recorded the evoked currents of hTRPA1(Y840F) (Fig. 4E) and hTRPA1(Y840W) (Fig. 4F). While THC evokes robust currents from the Y840F mutation (similar to the wt receptor), no current was evoked from the Y840W substitution (Fig. 4G). Moreover, the Y840F substitution significantly affects the CBD-evoked current response (Suppl. Fig. 4). Hence, our docking model and its analysis indicate that although both cannabinoids bind to the GNE551 binding site, each cannabinoid interacts differently in this binding site.

3.4. CBD activation of TRPA1 also requires the general anesthetic binding site

In contrast to THC, in which only mutations in the GNE551 binding site affect its activity (Figs. 2B-C and 4), we found that CBD is also affected by mutation in the previously suggested general anesthetic (GA) binding site (M953A; Fig. 2A & 2D-E). Hence, we performed a docking analysis of CBD in the GA-binding site (Fig. 5A), using Induced-Fit docking simulations to take into account the flexibility of the binding site residues. According to our model, the side chain of M953 shapes the binding site and directly interacts with the cyclohexene ring of the CBD (Fig. 5A). To test the contribution of each binding site (i.e., GNE551 and GA) to the CBD activation of hTRPA1, we analyzed the evoked response of the mutations Y840W, M953A, and Y840W/M953A (Fig. 5B-C). Because the saturating concentration of 50 μM CBD (Fig. 1B) demonstrated a significantly hampered response of both single-point mutations (i.e., Y840W and M953A) (Fig. 2E), we used an over-saturating concentration of CBD (100 μM) to test the involvement of each binding site. Of note, higher concentrations of CBD (or THC) were avoided due to salting out of the compounds in high concentrations. We found that

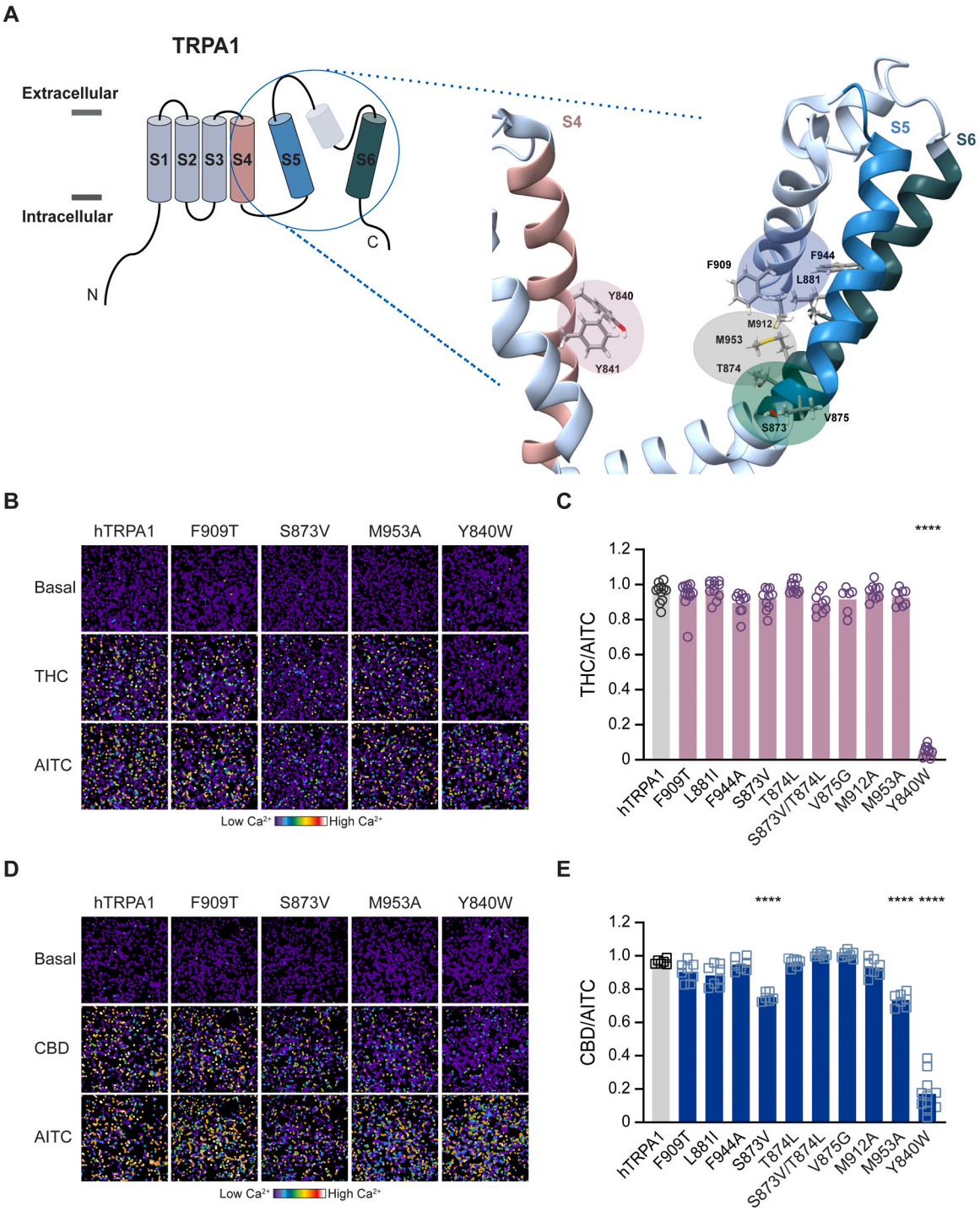

Fig. 2. THC and CBD have distinct binding mechanisms. A. Schematic structure of the TRPA1 channels, containing six transmembrane domains and intracellular N- and C-terminals. ***Right panel***, side view of the S4-S6 region (modified from PDB ID:6X2J) consisting of the main residues previously suggested to participate in the binding of non-electrophilic ligands. The residues are shown in balls & sticks with oxygen atoms in red and sulfur atoms in yellow, and the protein in light grey cartoon style (S4: light pink, S5: blue, and S6: green). Oval shapes present the different suggested binding domains of non-electrophilic ligands. Oval blue: part of the antagonist A967079 binding site; Oval green: part of the agonist's menthol, thymol, and carvacrol binding site; Oval green and grey: part of the general anesthetics binding site; Oval pink: part of the agonists β-eudesmol and the GNE551 binding sites. **B and D**. Representative pseudo-colored images of HEK293T cells transiently expressing hTRPA1 (left panels) or TRPA1 allosteric binding site mutated receptors after application of THC (**B**, 50 μM) or CBD (**D**, 50 μM) followed by applying AITC (50 μM). The scale bar indicates levels of intracellular calcium. **C and E.** Scatter dot plot shows THC (**C**, purple circles, light pink bars) or CBD (**E**, light blue squares, blue bars) evoked calcium response of HEK293T cells transiently expressing wt hTRPA1(black circles (**C**) or black squares **(E)** grey bars), or a mutated receptor, normalized to AITC evoked response. Data represent mean, N = 7–13 independent experiments, $n \geq 50$ cells per transfection condition per experiment. Statistical significance between responses of hTRPA1 and mutated receptor was determined using ordinary one-way ANOVA followed by a multiple comparison test when only statistically significant differences are indicated. ****, $p \leq 0.0001$.

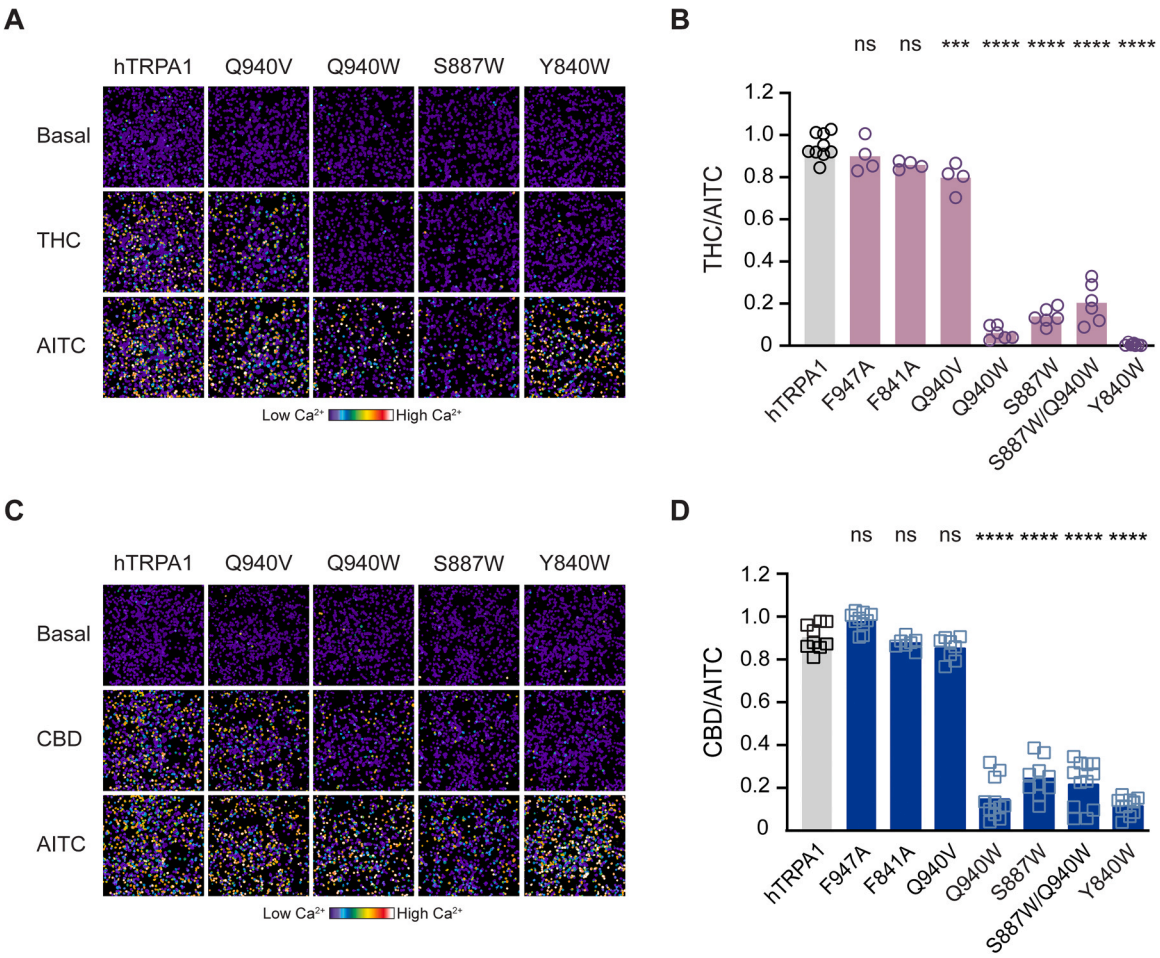

Fig. 3. THC and CBD activate TRPA1 through the GNE551 binding site. A. Representative pseudo-colored images of HEK293T cells transiently expressing wt hTRPA1 (**left panels**) or GNE551 binding site mutated receptors after application of THC (30 μM) followed by applying AITC (300 μM). The scale bar indicates levels of intracellular calcium. **B.** Scatter dot plot shows THC (30 μM)-evoked calcium response of HEK293T cells transiently expressing wt hTRPA1(grey bar, black circles), the GNE551 binding site mutated receptors (light pink bars, purple circles), normalized to AITC (300 μM) evoked response. Data represent mean, N = 4–9 independent experiments, n ≥ 50 cells per transfection condition per experiment. Statistical significance between responses compared to hTRPA1(wt) was determined using ordinary one-way ANOVA followed by a multiple comparison test when ***, $p \leq 0.001$, ****, $p \leq 0.0001$, and ns are not statistically significant. **C.** Representative pseudo-colored images of HEK293T cells transiently expressing wt hTRPA1 (**left panels**) or GNE551 binding site mutated receptors after application of CBD (30 μM) followed by applying AITC (300 μM). The scale bar indicates levels of intracellular calcium. **D.** Scatter dot plot shows CBD (30 μM)-evoked calcium response of HEK293T cells transiently expressing wt hTRPA1(grey bar, black squares), the GNE551 binding site mutated receptors (blue bars, light blue squares), normalized to AITC (300 μM)-evoked response. Data represent mean, N = 7–12 independent experiments, n ≥ 50 cells per transfection condition per experiment. Statistical significance between responses compared to hTRPA1(wt) was determined using ordinary one-way ANOVA followed by a multiple comparison test when ****, $p \leq 0.0001$, and ns, are not statistically significant.

while the single-point mutants significantly reduced the CBD-evoked response, the double mutation (Y840W/M953A) dramatically diminished it (Fig. 5C). To better analyze the role of each binding site in the activation of CBD, we recorded the evoked current of the different constructs (Fig. 5D-H). Similar to our results in calcium imaging, both binding sites are required for the CBD activation in over-saturating concentration (Fig. 5F, G &H). Importantly, in negative potentials, the double mutation abolished the CBD response (Fig. 5F). Of note, in contrast to CBD, over-saturating concentration of THC (100 μM) does not increase the response of the Y840W mutation (Suppl. Fig. 5). To further verify our results, we generate four 2D ligand interaction diagrams for THC and CBD in the GNE551 and GA binding sites (Suppl. Fig. 6), and analyzed each residue that is shown to interact with the agonists (Suppl. Table.2). Our results demonstrate that both THC and CBD bind to the GNE551 binding site, as mutations of multiple residues affect the agonists' responses. On the other hand, while none of the mutations in the site of the GA affect THC, multiple residues affect the CBD response. Therefore, our finding indicated that while THC response is mediated through the GNE551 binding site, the CBD response may be evoked from both the GNE551 and the GA binding sites.

4. Discussion

TRPA1 is a chemosensor with a variety of ligands and multiple activation mechanisms [14,16–18,20]. While its unorthodox activation by electrophilic compounds was thoroughly investigated [20–22], TRPA1 activation by non-electrophilic compounds is yet to be fully resolved [23,44]. Here, we investigate the activation mechanism of TRPA1 by the phytocannabinoids THC and CBD. Although these compounds were used for the original cloning of TRPA1 and were the first activators to be described as non-electrophilic agonists [11,20], their binding site is yet to be defined. Our results indicate that both cannabinoids have similar activation profiles (Fig. 1). Considering that both are phytocannabinoids, have similar hydrophobicity/lipophilicity [45,46], with similar potency and efficacy (Fig. 1A-D and Suppl. Fig. 1B, C & E), and do not bind to the electrophilic binding site (Fig. 1E-F, and Suppl. Fig. 1F) [20], we hypothesized that both compounds have the same binding site(s). Using site-directed mutagenesis of hTRPA1 and calcium

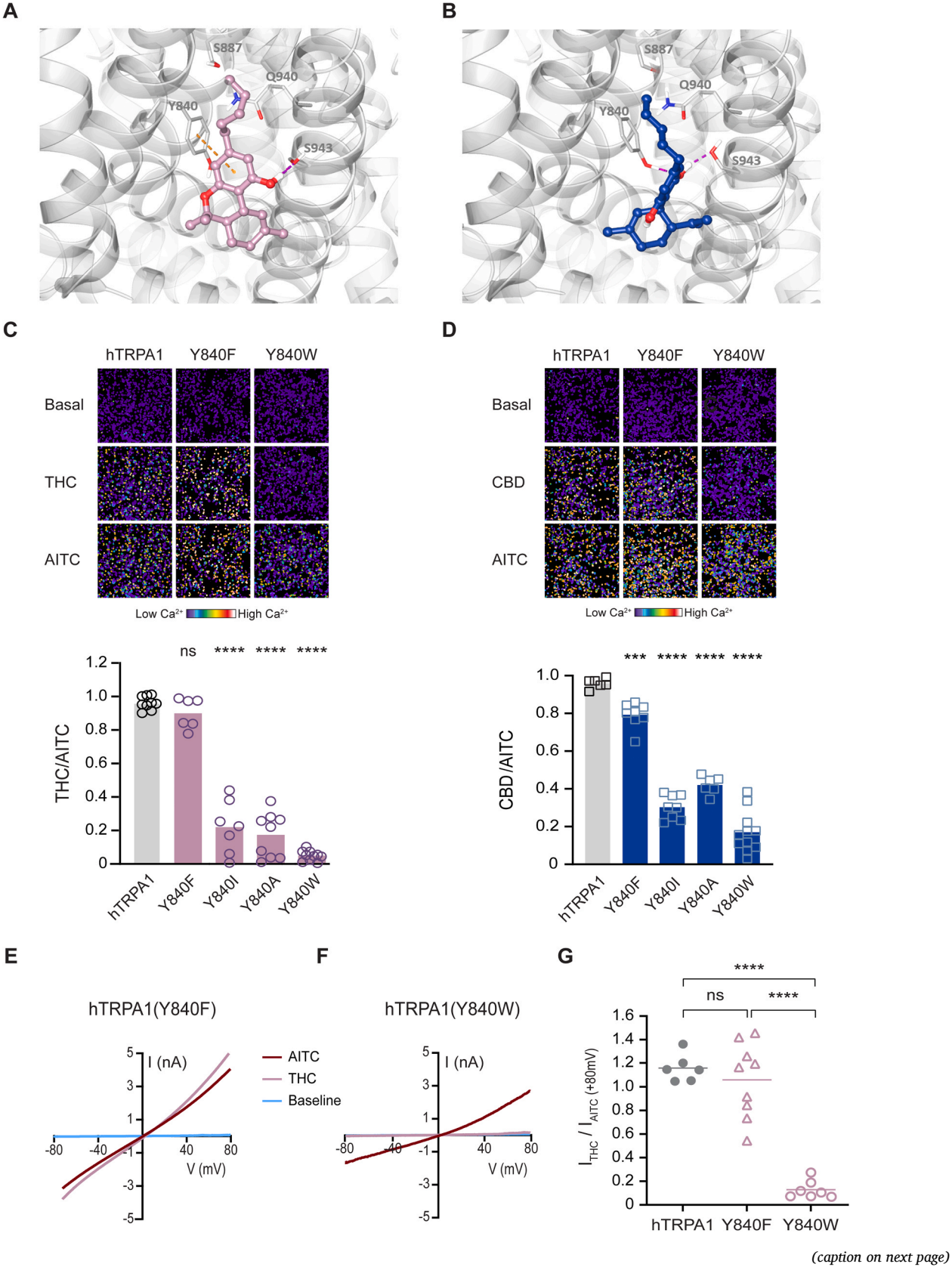

(caption on next page)

Fig. 4. A key role of Y840 in the hTRPA1 interaction with CBD and THC. A. Putative binding mode of THC in the GNE551 binding site. The ligand is shown in CPK balls & sticks with carbon atoms in pink, the protein in light grey cartoon style. Y840, S887, Q940, and S943 are represented as sticks. **B.** Putative binding mode of CBD in the GNE551 binding site.The ligand is shown in CPK balls & sticks with carbon atoms in blue, the protein in light grey cartoon style. Y840, S887, Q940, and S943 are represented as sticks. **C. (upper panel);** Representative pseudo-colored images of HEK293T cells transiently expressing wt hTRPA1(**left panel**) and the Y840F (**middle panel**) or Y840W (**right panel**) mutated receptors after application of THC (50 μM) followed by applying AITC (50 μM). The scale bar indicates levels of intracellular calcium. **(bottom panel);** Scatter dot plot shows THC (50 μM)-evoked calcium response of HEK293T cells transiently expressing wt hTRPA1 (grey bar, black circles) or receptors mutated at Y840 (Y840F, Y840I, Y840A, and Y840W) (light pink bars, purple circles), normalized to AITC (50 μM)-evoked response. Data represent mean, N = 6–10 independent experiments, n ≥ 50 cells per transfection condition per experiment. Statistical significance between responses compared to hTRPA1(wt) was determined using ordinary one-way ANOVA followed by a multiple comparison test when ****, $p \leq 0.0001$, and ns, are not statistically significant. **D. (upper panel);** Representative pseudo-colored images of HEK293T cells transiently expressing wt hTRPA1(**left panel**) and the Y840F (**middle panel**) or Y840W (**right panel**) mutated receptors after application of CBD (50 μM) followed by applying AITC (50 μM). The scale bar indicates levels of intracellular calcium. **(bottom panel);** Scatter dot plot shows CBD (50 μM)-evoked calcium response of HEK293T cells transiently expressing wt hTRPA1(grey bar, black squares) or receptors mutated at Y840 (Y840F, Y840I, Y840A, and Y840W) (blue bars, light blue squares), normalized to AITC (50 μM)-evoked response. Data represent mean, N = 6–11 independent experiments, n ≥ 50 cells per transfection condition per experiment. Statistical significance between responses compared to hTRPA1(wt) was determined using ordinary one-way ANOVA followed by a multiple comparison test when ***, $p \leq 0.001$, ****, $p \leq 0.0001$, and ns, are not statistically significant. **E and F.** Representative current-voltage relationship traces in HEK293T cells transiently expressing hTRPA1(Y840F) (**E**) and hTRPA1(Y840W) (**F**) before (light blue line; Baseline) and after exposure to THC (50 μM, light pink line) followed by AITC (50 μM, dark red line) application. Currents were recorded using whole-cell patch-clamp recording (1 s^{-1} voltage ramps between −80 and +80 mV). **G** Mean/scatter-dot plot representing the ratio between THC (50 μM)-evoked current to that evoked by AITC (50 μM) in HEK293T cells transiently expressing wt hTRPA1(grey circles), hTRPA1 (Y840F);(light pink triangle) and hTRPA1 (Y840W);(light pink circles). Currents were recorded using whole-cell patch-clamp recording (1 s^{-1} voltage ramps between −80 and +80 mV), representing the current amplitudes at +80 mV (n = 6–8). Statistical significance between responses compared to hTRPA1(wt) or comparison between mutations hTRPA1(Y840F) and hTRPA1(Y840W) was determined using ordinary one-way ANOVA followed by a multiple comparison test when ****, $p \leq 0.0001$ and ns, are not statistically significant.

imaging, electrophysiology, and molecular modeling, we screened residues that were previously shown to participate in the binding of non-electrophilic modulators (Fig. 2). We found that mutagenesis of residue Y840 was sufficient to abolish the THC and CBD response at saturating concentrations (Fig. 3 & 4). Also, we found that other residues that were shown to participate in the binding of GNE551 affect the binding of both cannabinoids (Fig. 3). While molecular modeling of THC and CBD docked in the GNE551 binding site reveals that both cannabinoids interact with Y840, the interaction is different (Fig. 4). Surprisingly, testing over-saturating concentration (100 μM) of both cannabinoids exposed another binding site for CBD (Fig. 5 and suppl. Fig. 5). Together, our results suggest that the cannabinoid-binding site (CBS) mainly overlapped with the previously suggested β-eudesmol [43] and GNE551 [30] binding site (compare Fig. 6 and Fig. 2A). CBD can also bind to the general anesthetic binding site [27] at high concentrations (Fig. 6). Thus, our findings suggest that TRPA1 has a specific binding site for cannabinoids. Furthermore, it has a highly flexible region to bind non-electrophilic activators, demonstrating the important role of this chemosensor in detecting noxious stimuli.

Previous studies investigated the cannabinoids' complex pharmacological and physiological roles, revealing a multifaceted interaction with the endocannabinoid system (ECS) and various ion channels, such as the TRPA1 [4,47,48]. The interaction with TRPA1 suggests that cannabinoids can modulate pain and inflammation pathways directly, independent of their actions on cannabinoid receptors [4,48]. Evidence that phytocannabinoids activate TRPA1 was first described in the TRPA1 cloning study [11,12]. Later, phyto- and endocannabinoids were shown to induce TRPA1-mediated Ca^{2+} elevation at different potencies, and they might exert anti-inflammatory and analgesic effects via TRPA1 activation/desensitization [2,4,5,9]. However, the TRPA1 activation mechanism by cannabinoids was still unknown; it is already described that these compounds do not activate the channel in a covalent, cysteine-dependent manner [20]. CBD and THC have potent TRPA1-activating properties (Fig. 1). In addition, CBD was shown to desensitize TRPA1 potently [17]. Although the exact physiological effect of cannabinoids on TRPA1 is not fully understood, our finding that the main phytocannabinoids in the plant activate the channel through defined CBS points to the importance of these processes. Moreover, phytocannabinoids are natural TRPA1 agonists. Hence, our results suggest that non-electrophilic activation of TRPA1 evolved for the specific physiological roles of this channel.

The dramatic effect of mutagenesis of residue Y840 on TRPA1 sensitivity to either THC or CBD was instrumental in suggesting that this region serves as the CBS (Fig. 3). By using molecular modeling of the previously published hTRPA1 in complex with the synthetic compound GNE551 [30], we show that the binding of cannabinoids in this site is feasible (Fig. 4A & 4B). However, our findings suggest that each cannabinoid interacts differently with the Y840 residue. While THC can establish a π−π stacking interaction, CBD generates a hydrogen bond with the phenolic hydroxide of the Y840. This finding points to the flexibility of the CBS in which each ligand may interact differently with the different determinants of the binding site to reach a similar effect (i.e., channel activation). Of note, similar results were also shown for the pain receptor TRPV1 regarding compounds that activate the channel through the vanilloid binding site (VBS) [49,50]. Nevertheless, the exact interaction and the different poses of cannabinoids in the TRPA1 CBS should be further analyzed using structure studies.

In contrast to our initial hypothesis that both phytocannabinoids activate TRPA1 through the same binding site, an over-saturating concentration (100 μM) of CBD reveals another putative binding site (Fig. 5). This low-affinity binding site was previously shown to act as the general anesthetic (GA) binding domain [28]. Of note, THC in all tested concentrations was only affected by the CBS mutagenesis (Figs. 2–4; Suppl. Figs. 3 and 5). A combination of mutagenesis in the GA binding site (M953A) and the CBS (Y840W) abolished the CBD-evoked response even in over-saturation concentrations (Fig. 5). Our finding that in close to EC_{50} concentration (i.e., 30 μM) (Fig. 3), the Y840W mutation was sufficient to abolish the CBD response point to the CBS as the primary binding site of cannabinoids. Nevertheless, we can not rule out that CBD activates the channel through both sites throughout the concentration range. The multiple-binding sites of CBD were previously shown for TRPV2 and $Na_V1.7$ [51,52]. Combined with our results, this may suggest that due to its chemical properties (e.g., hydrophobicity, another hydroxyl group) and shape, CBD can bind to multiple binding domains in different affinities. This may also explain the variety of suggested targets for CBD therapeutic effects [31]. Hence, defining the binding site for CBD should be corroborated with functional analysis and not solely rely on structural determination. Our results suggest that while both THC and CBD activate TRPA1 through the CBS throughout the dose-response relation curve, only CBD in over-saturating concentration can partially activate the channel through the GA domain (Fig. 6). This result may be due to the promiscuity of CBD rather than the specific interaction between the receptor and its agonist.

Although the mechanism of action underlying the analgesic effect of phytocannabinoids is yet to be resolved, these compounds' direct effects on receptors/channels specific to the pain system may substantially contribute to this process. Thus, defining the cannabinoids binding site of the major cannabinoids (THC and CBD) in the pain receptor, TRPA1,

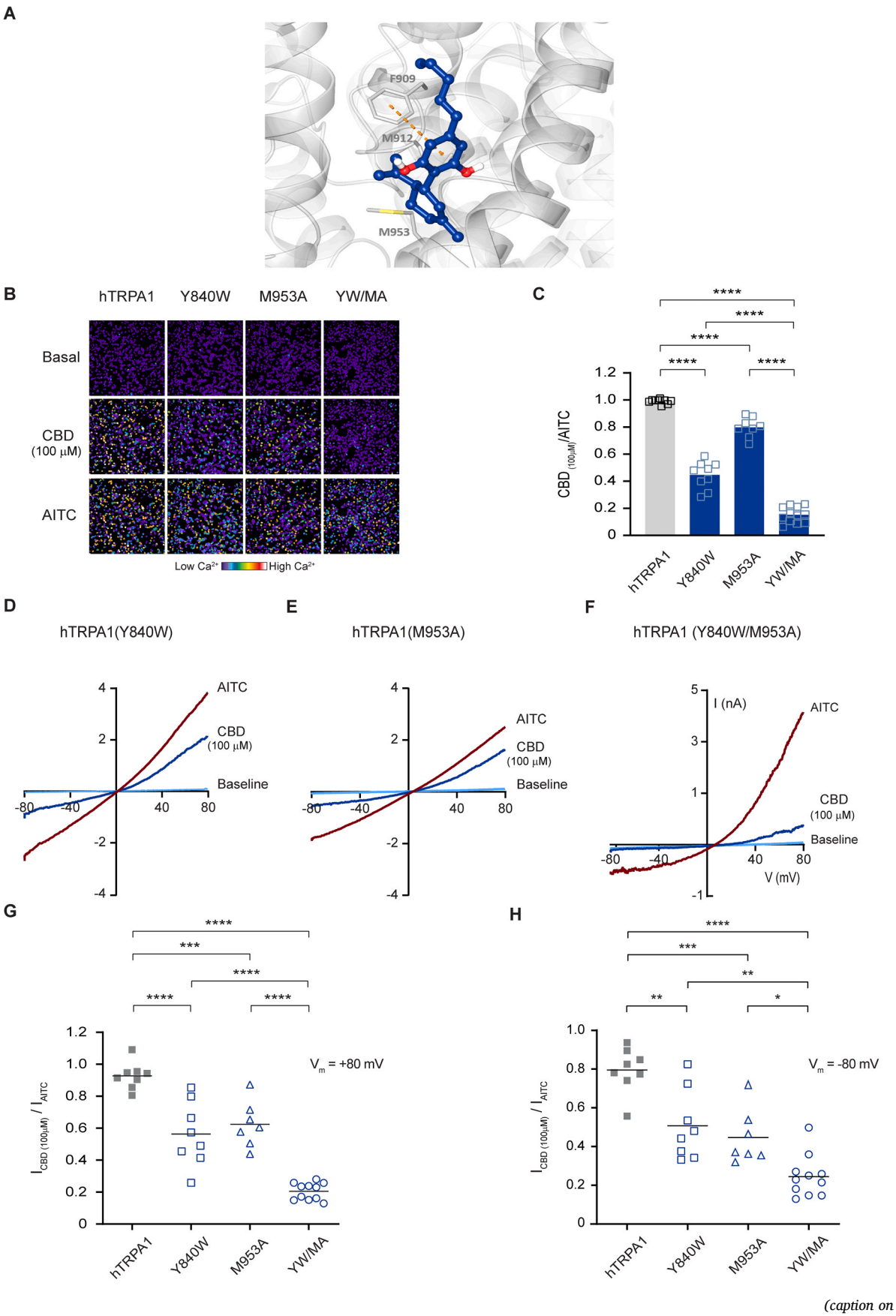

(caption on next page)

Fig. 5. Two binding domains govern the CBD-evoked TRPA1 activation. A. Putative binding mode of CBD in the general anesthetics binding site. The ligand is shown in CPK balls & sticks with carbon atoms in blue, the protein in light grey cartoon style. F909, M912, and M953 are represented as sticks. **B.** Representative pseudo-colored images of HEK293T cells transiently expressing wt hTRPA1 (*left panel*) and the Y840W (*left middle panel*), M953A (*right middle panel*) or Y840W/M953A (*right panel*) mutated receptors after application of CBD (100 μM) followed by applying AITC (50 μM). The scale bar indicates levels of intracellular calcium. **C.** Scatter dot plot shows CBD (100 μM)-evoked calcium response of HEK293T cells transiently expressing wt hTRPA1(grey bar, black squares) or receptors mutated (Y840W, M953A, and Y840W/M953A) (blue bars, light blue squares), normalized to AITC (50 μM)-evoked response. Data represent mean, N = 8–12 independent experiments, n ≥ 50 cells per transfection condition per experiment. Statistical significance between responses compared to hTRPA1(wt) or comparison between the mutations was determined using ordinary one-way ANOVA followed by a multiple comparison test when ***, $p \leq 0.001$, ****, $p \leq 0.0001$. **D, E and F.** Representative current-voltage relationship traces in HEK293T cells transiently expressing (**D**): hTRPA1(Y840W) (**E**): hTRPA1(M953A), (**F**): hTRPA1(Y840W/M953A) before (light blue line; Baseline) and after exposure to CBD (100 μM, blue line) followed by AITC (50 μM, dark red line) application. Currents were recorded using whole-cell patch-clamp recording (1 s^{-1} voltage ramps between −80 and +80 mV). **G and H.** Mean/scatter-dot plot representing the ratio between CBD (100 μM)-evoked current to that evoked by AITC (50 μM) in HEK293T cells transiently expressing wt hTRPA1(grey squares); hTRPA1(Y840W) (blue squares); hTRPA1(M953A) (blue triangles); and hTRPA1(Y840W/M953A) (blue circles). Currents were recorded using whole-cell patch-clamp recording (1 s^{-1} voltage ramps between −80 and +80 mV), representing the current amplitudes (**G**) at +80 mV (n = 7–11) and (H) at −80 mV (n = 7–11). Statistical significance between responses compared to hTRPA1(wt) or comparison between the mutations was determined using ordinary one-way ANOVA followed by a multiple comparison test when *, $p \leq 0.1$, **, $p \leq 0.01$ ***, $p \leq 0.001$, ****, $p \leq 0.0001$.

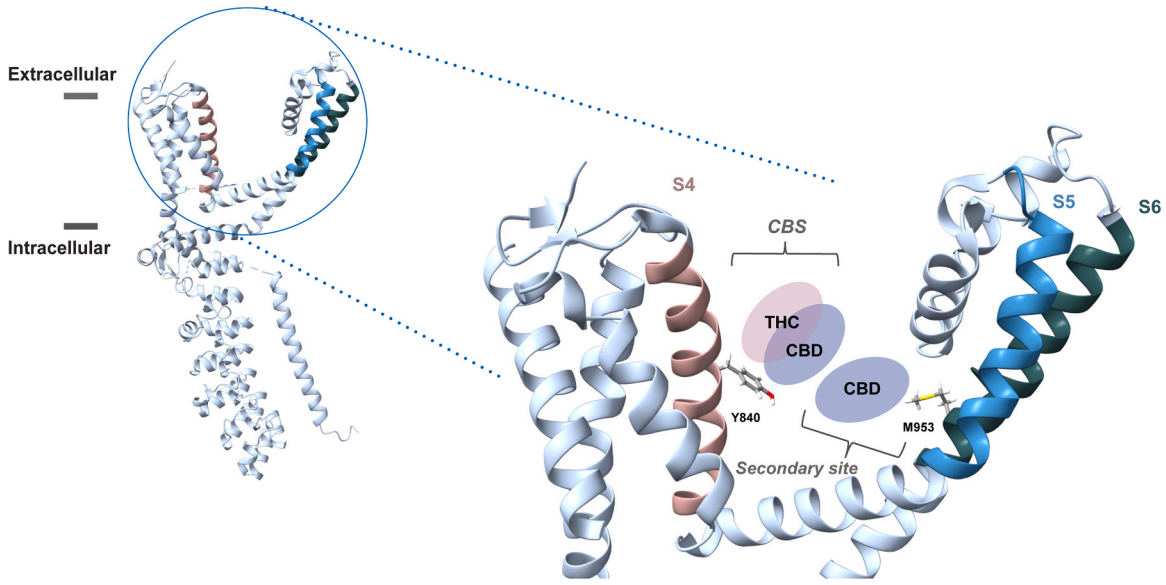

Fig. 6. Schematic model of the cannabinoids binding sites. ***Left panel***, Ribbon diagram depicting a side view of the TRPA1 subunit based on PDB ID:6X2J. ***Right panel***, zoom in to our suggested CBS domain. Both THC (oval pink) and CBD (oval blue) interact with the Y840 in S4. CBD also binds to a secondary site in S6. The residues are shown in balls and stick with oxygen atoms in red and sulfur atoms in yellow, and the protein in a light grey cartoon style (S4: light pink, S5: blue, and S6: green).

should enable a better understating of the chemosensation of the pain pathway and the development of phytocannabinoid-based drugs for analgesia.

CRediT authorship contribution statement

Tala Amawi: Writing – original draft, Investigation, Formal analysis, Data curation. **Avi Priel:** Writing – original draft, Supervision, Resources, Project administration, Investigation, Funding acquisition, Formal analysis, Conceptualization. **Antonella Di Pizio:** Writing – original draft, Supervision, Funding acquisition, Formal analysis, Data curation. **Masha Y Niv:** Supervision, Funding acquisition. **Mariana Ghantous:** Formal analysis, Data curation. **Gilad Noy:** Data curation. **Alaa Nmarneh:** Formal analysis, Data curation.

Declaration of Competing Interest

None.

Acknowledgments

We thank the A.P. laboratory members for their insightful comments and for critically reading the manuscript. This work was funded by The Israel Science Foundation (ISF) – Individual Research grant 2136/20 (to A.P.) and 1129/19 (to M.Y.N.), the Leibniz Programme for Women Professors grant P116/2020 (to A.D.P.), the Israel Cancer Research Fund (ICRF) – The Brause Family Initiative for Quality of Life 22-402-QOL (to A.P.), and the Brettler Center, and the David R. Bloom Center of the School of Pharmacy (The Hebrew University of Jerusalem; to A.P.).

Appendix A. Supporting information

Supplementary data associated with this article can be found in the online version at doi:10.1016/j.phrs.2024.107444.

References

[1] K.F. Boehnke, C.L. Wu, D.J. Clauw, Thoughtfully integrating cannabis products into chronic pain treatment, Anesth. Analg. 138 (2024) 5–15, https://doi.org/10.1213/ANE.0000000000005904.
[2] C. Muller, P. Morales, P.H. Reggio, Cannabinoid ligands targeting TRP channels, Front Mol. Neurosci. 11 (2018) 487, https://doi.org/10.3389/fnmol.2018.00487.
[3] J.H. Khalsa, G. Bunt, K. Blum, S.B. Maggirwar, M. Galanter, M.N. Potenza, Review: cannabinoids as medicinals, Curr. Addict. Rep. 9 (2022) 630–646, https://doi.org/10.1007/s40429-022-00438-3.
[4] L. De Petrocellis, A. Ligresti, A.S. Moriello, M. Allarà, T. Bisogno, S. Petrosino, et al., Effects of cannabinoids and cannabinoid-enriched Cannabis extracts on TRP

channels and endocannabinoid metabolic enzymes, Br. J. Pharm. 163 (2011) 1479–1494, https://doi.org/10.1111/j.1476-5381.2010.01166.x.
[5] L. Etemad, G. Karimi, M.S. Alavi, A. Roohbakhsh, Pharmacological effects of cannabidiol by transient receptor potential channels, Life Sci. 300 (2022) 120582, https://doi.org/10.1016/j.lfs.2022.120582.
[6] I. Jardín, J.J. López, R. Diez, J. Sánchez-Collado, C. Cantonero, L. Albarrán, et al., Trps in pain sensation, Front Physiol. 8 (2017) 392, https://doi.org/10.3389/fphys.2017.00392.
[7] D. Julius, TRP channels and pain, Annu Rev. Cell Dev. Biol. 29 (2013) 355–384, https://doi.org/10.1146/annurev-cellbio-101011-155833.
[8] Y. Lee, C.-H. Lee, U. Oh, Painful channels in sensory neurons, Mol. Cells 20 (2005) 315–324, https://doi.org/10.1016/S1016-8478(23)25242-5.
[9] L. De Petrocellis, V. Vellani, A. Schiano-Moriello, P. Marini, P.C. Magherini, P. Orlando, et al., Plant-derived cannabinoids modulate the activity of transient receptor potential channels of ankyrin type-1 and melastatin type-8, J. Pharm. Exp. Ther. 325 (2008) 1007–1015, https://doi.org/10.1124/jpet.107.134809.
[10] E.J. Cavanaugh, D. Simkin, D. Kim, Activation of transient receptor potential A1 channels by mustard oil, tetrahydrocannabinol and Ca2+ reveals different functional channel states, Neuroscience 154 (2008) 1467–1476, https://doi.org/10.1016/j.neuroscience.2008.04.048.
[11] S.-E. Jordt, D.M. Bautista, H.-H. Chuang, D.D. McKemy, P.M. Zygmunt, E. D. Högestätt, et al., Mustard oils and cannabinoids excite sensory nerve fibres through the TRP channel ANKTM1, Nature 427 (2004) 260–265, https://doi.org/10.1038/nature02282.
[12] G.M. Story, A.M. Peier, A.J. Reeve, S.R. Eid, J. Mosbacher, T.R. Hricik, et al., ANKTM1, a TRP-like channel expressed in nociceptive neurons, is activated by cold temperatures, Cell 112 (2003) 819–829, https://doi.org/10.1016/s0092-8674(03)00158-2.
[13] J. Chen, D.H. Hackos, TRPA1 as a drug target–promise and challenges. Naunyn Schmiede Arch. Pharm. 388 (2015) 451–463, https://doi.org/10.1007/s00210-015-1088-3.
[14] K. Nagata, A. Duggan, G. Kumar, J. García-Añoveros, Nociceptor and hair cell transducer properties of TRPA1, a channel for pain and hearing, J. Neurosci. 25 (2005) 4052–4061, https://doi.org/10.1523/JNEUROSCI.0013-05.2005.
[15] T.I. Kichko, W. Neuhuber, G. Kobal, P.W. Reeh, The roles of TRPV1, TRPA1 and TRPM8 channels in chemical and thermal sensitivity of the mouse oral mucosa, Eur. J. Neurosci. 47 (2018) 201–210, https://doi.org/10.1111/ejn.13799.
[16] E.S. Fernandes, M.A. Fernandes, J.E. Keeble, The functions of TRPA1 and TRPV1: moving away from sensory nerves, Br. J. Pharm. 166 (2012) 510–521, https://doi.org/10.1111/j.1476-5381.2012.01851.x.
[17] J.E. Meents, C.I. Ciotu, M.J.M. Fischer, TRPA1: a molecular view, J. Neurophysiol. 121 (2019) 427–443, https://doi.org/10.1152/jn.00524.2018.
[18] B. Nilius, G. Appendino, G. Owsianik, The transient receptor potential channel TRPA1: from gene to pathophysiology, Pflug. Arch. 464 (2012) 425–458, https://doi.org/10.1007/s00424-012-1158-z.
[19] A. Samanta, T.E.T. Hughes, V.Y. Moiseenkova-Bell, Transient receptor potential (TRP) channels, Subcell. Biochem 87 (2018) 141–165, https://doi.org/10.1007/978-981-10-7757-9_6.
[20] A. Hinman, H.-H. Chuang, D.M. Bautista, D. Julius, TRP channel activation by reversible covalent modification, Proc. Natl. Acad. Sci. USA 103 (2006) 19564–19568, https://doi.org/10.1073/pnas.0609598103.
[21] M.S.J. Brewster, R. Gaudet, How the TRPA1 receptor transmits painful stimuli: Inner workings revealed by electron cryomicroscopy, Bioessays 37 (2015) 1184–1192, https://doi.org/10.1002/bies.201500085.
[22] Y. Suo, Z. Wang, L. Zubcevic, A.L. Hsu, Q. He, M.J. Borgnia, et al., Structural insights into electrophile irritant sensing by the human TRPA1 channel, Neuron 105 (2020) 882–894.e5, https://doi.org/10.1016/j.neuron.2019.11.023.
[23] S. Saito, M. Tominaga, Evolutionary tuning of TRPA1 and TRPV1 thermal and chemical sensitivity in vertebrates, Temperature 4 (2017) 141–152, https://doi.org/10.1080/23328940.2017.1315478.
[24] J. Zhao, J.V. Lin King, C.E. Paulsen, Y. Cheng, D. Julius, Irritant-evoked activation and calcium modulation of the TRPA1 receptor, Nature 585 (2020) 141–145, https://doi.org/10.1038/s41586-020-2480-9.
[25] G. Klement, L. Eisele, D. Malinowsky, A. Nolting, M. Svensson, G. Terp, et al., Characterization of a ligand binding site in the human transient receptor potential ankyrin 1 pore, Biophys. J. 104 (2013) 798–806, https://doi.org/10.1016/j.bpj.2013.01.008.
[26] N. Banzawa, S. Saito, T. Imagawa, M. Kashio, K. Takahashi, M. Tominaga, et al., Molecular basis determining inhibition/activation of nociceptive receptor TRPA1 protein: a single amino acid dictates species-specific actions of the most potent mammalian TRPA1 antagonist, J. Biol. Chem. 289 (2014) 31927–31939, https://doi.org/10.1074/jbc.M114.586891.
[27] H.T. Ton, T.X. Phan, A.M. Abramyan, L. Shi, G.P. Ahern, Identification of a putative binding site critical for general anesthetic activation of TRPA1, Proc. Natl. Acad. Sci. USA 114 (2017) 3762–3767, https://doi.org/10.1073/pnas.1618144114.
[28] B. Xiao, A.E. Dubin, B. Bursulaya, V. Viswanath, T.J. Jegla, A. Patapoutian, Identification of transmembrane domain 5 as a critical molecular determinant of menthol sensitivity in mammalian TRPA1 channels, J. Neurosci. 28 (2008) 9640–9651, https://doi.org/10.1523/JNEUROSCI.2772-08.2008.
[29] Y. Karashima, N. Damann, J. Prenen, K. Talavera, A. Segal, T. Voets, et al., Bimodal action of menthol on the transient receptor potential channel TRPA1, J. Neurosci. 27 (2007) 9874–9884, https://doi.org/10.1523/JNEUROSCI.2221-07.2007.
[30] C. Liu, R. Reese, S. Vu, L. Rougé, S.D. Shields, S. Kakiuchi-Kiyota, et al., A non-covalent ligand reveals biased agonism of the TRPA1 ion channel, Neuron 109 (2021) 273–284.e4, https://doi.org/10.1016/j.neuron.2020.10.014.
[31] J. Peng, M. Fan, C. An, F. Ni, W. Huang, J. Luo, A narrative review of molecular mechanism and therapeutic effect of cannabidiol (CBD), Basic Clin. Pharm. Toxicol. 130 (2022) 439–456, https://doi.org/10.1111/bcpt.13710.
[32] A. Hazan, R. Kumar, H. Matzner, A. Priel, The pain receptor TRPV1 displays agonist-dependent activation stoichiometry, Sci. Rep. 5 (2015) 12278, https://doi.org/10.1038/srep12278.
[33] C.J. Bohlen, A. Priel, S. Zhou, D. King, J. Siemens, D. Julius, A bivalent tarantula toxin activates the capsaicin receptor, TRPV1, by targeting the outer pore domain, Cell 141 (2010) 834–845, https://doi.org/10.1016/j.cell.2010.03.052.
[34] A. Priel, S. Selak, J. Lerma, Y. Stern-Bach, Block of kainate receptor desensitization uncovers a key trafficking checkpoint, Neuron 52 (2006) 1037–1046, https://doi.org/10.1016/j.neuron.2006.12.006.
[35] A. Zagzoog, K.A. Mohamed, H.J.J. Kim, E.D. Kim, C.S. Frank, T. Black, et al., In vitro and in vivo pharmacological activity of minor cannabinoids isolated from Cannabis sativa, Sci. Rep. 10 (2020) 20405, https://doi.org/10.1038/s41598-020-77175-y.
[36] N. Pintori, F. Caria, M.A. De Luca, C. Miliano, THC and CBD: villain versus Hero? Insights into adolescent exposure, Int J. Mol. Sci. 24 (2023), https://doi.org/10.3390/ijms24065251.
[37] M.J. López-González, E. Luis, O. Fajardo, V. Meseguer, K. Gers-Barlag, S. Niñerola, et al., TRPA1 channels mediate human gingival fibroblast response to phenytoin, J. Dent. Res 96 (2017) 832–839, https://doi.org/10.1177/0022034517695518.
[38] X. Wan, Y. Lu, X. Chen, J. Xiong, Y. Zhou, P. Li, et al., Bimodal voltage dependence of TRPA1: mutations of a key pore helix residue reveal strong intrinsic voltage-dependent inactivation, Pflug. Arch. 466 (2014) 1273–1287, https://doi.org/10.1007/s00424-013-1345-6.
[39] M.J.M. Fischer, D. Balasuriya, P. Jeggle, T.A. Goetze, P.A. McNaughton, P.W. Reeh, et al., Direct evidence for functional TRPV1/TRPA1 heteromers, Pflug. Arch. 466 (2014) 2229–2241, https://doi.org/10.1007/s00424-014-1497-z.
[40] S. Giorgi, M. Nikolaeva-Koleva, D. Alarcón-Alarcón, L. Butrón, S. González-Rodríguez, Is TRPA1 burning down TRPV1 as druggable target for the treatment of chronic pain? Int J. Mol. Sci. 20 (2019) https://doi.org/10.3390/ijms20122906.
[41] K.V. Torres, S. Pantke, D. Rudolf, M.M. Eberhardt, A. Leffler, The coumarin osthole is a non-electrophilic agonist of TRPA1, Neurosci. Lett. 789 (2022) 136878, https://doi.org/10.1016/j.neulet.2022.136878.
[42] K. Nakatsuka, R. Gupta, S. Saito, N. Banzawa, K. Takahashi, M. Tominaga, et al., Identification of molecular determinants for a potent mammalian TRPA1 antagonist by utilizing species differences, J. Mol. Neurosci. 51 (2013) 754–762, https://doi.org/10.1007/s12031-013-0060-2.
[43] K. Ohara, T. Fukuda, H. Okada, S. Kitao, Y. Ishida, K. Kato, et al., Identification of significant amino acids in multiple transmembrane domains of human transient receptor potential ankyrin 1 (TRPA1) for activation by eudesmol, an oxygenized sesquiterpene in hop essential oil, J. Biol. Chem. 290 (2015) 3161–3171, https://doi.org/10.1074/jbc.M114.600932.
[44] R. Gupta, S. Saito, Y. Mori, S.G. Itoh, H. Okumura, M. Tominaga, Structural basis of TRPA1 inhibition by HC-030031 utilizing species-specific differences, Sci. Rep. 6 (2016) 37460, https://doi.org/10.1038/srep37460.
[45] C.J. Lucas, P. Galettis, J. Schneider, The pharmacokinetics and the pharmacodynamics of cannabinoids, Br. J. Clin. Pharm. 84 (2018) 2477–2482, https://doi.org/10.1111/bcp.13710.
[46] Thomas B., Compton D., Martin B. Characterization of the Lipophilicity of Natural and Synthetic Analogs of L\9-Tetrahydrocannabinol and Its Relationship to Pharmacological Potency1 n.d.
[47] V. Di Marzo, F. Piscitelli, The endocannabinoid system and its modulation by phytocannabinoids, Neurotherapeutics 12 (2015) 692–698, https://doi.org/10.1007/s13311-015-0374-6.
[48] A. Ligresti, L. De Petrocellis, V. Di Marzo, From phytocannabinoids to cannabinoid receptors and endocannabinoids: pleiotropic physiological and pathological roles through complex pharmacology, Physiol. Rev. 96 (2016) 1593–1659, https://doi.org/10.1152/physrev.00002.2016.
[49] V. Carnevale, T. Rohacs, TRPV1: a target for rational drug design, Pharmaceuticals 9 (2016), https://doi.org/10.3390/ph9030052.
[50] M.V. Yelshanskaya, A.I. Sobolevsky, Ligand-binding sites in vanilloid-subtype TRP channels, Front Pharm. 13 (2022) 900623, https://doi.org/10.3389/fphar.2022.900623.
[51] S. Feng, R.A. Pumroy, A.D. Protopopova, V.Y. Moiseenkova-Bell, W. Im, Modulation of TRPV2 by endogenous and exogenous ligands: a computational study, Protein Sci. 32 (2023) e4490, https://doi.org/10.1002/pro.4490.
[52] J. Huang, X. Fan, X. Jin, S. Jo, H.B. Zhang, A. Fujita, et al., Cannabidiol inhibits Nav channels through two distinct binding sites, Nat. Commun. 14 (2023) 3613, https://doi.org/10.1038/s41467-023-39307-6.